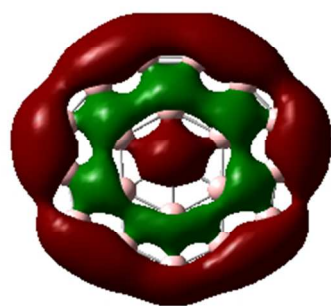


**Quantum rules for planar boron nanoclusters**

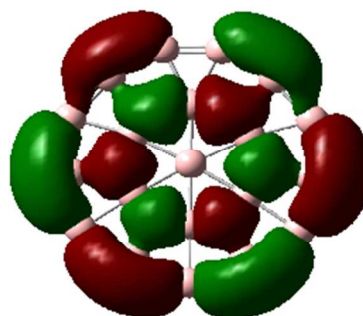
Journal:	<i>Physical Chemistry Chemical Physics</i>
Manuscript ID:	CP-ART-05-2014-002323.R2
Article Type:	Paper
Date Submitted by the Author:	16-Jul-2014
Complete List of Authors:	Arvanitidis, Athanasios; KU Leuven, Quantum Chemistry and Physical Chemistry Section Tai, Truong; Katholieke Universiteit Leuven, Chemistry Nguyen, M; Katholieke Universeit Leuven, Department of Chemistry Ceulemans, Arnout; Katholieke Universiteit Leuven, Chemistry

SCHOLARONE™  
Manuscripts

The nodal structure of boron sheets follows the pattern of cylindrical bessel function



$3\sigma$   
HOMO-13



$2\varphi$   
HOMO-8

# Quantum rules for planar boron nanoclusters

Cite this: DOI: 10.1039/x0xx00000x

Athanasios G. Arvanitidis,<sup>a</sup> Truong Ba Tai,<sup>a</sup> Minh Tho Nguyen,<sup>a</sup> and Arnout Ceulemans<sup>a</sup>

Received 00th May 2014,  
Accepted 00th May 2014

DOI: 10.1039/x0xx00000x

www.rsc.org/

This article presents the use of free particle models to obtain quantum rules for planar boron clusters, with nuclearities in the range from seven to twenty. The information obtained from the models is being compared with electronic structure calculations based on the DFT method. Separate rules for in-plane and out-of-plane bonding are derived. In-plane bonding is precise on the cluster boundary and forms a network of alternating triangular 3c-2e bonds on the inside. The out-of-plane bonding is strongly delocalized and only depends on the global shape and size of the cluster.

## 1. Introduction

In quantum systems boundary conditions are responsible for quantization of eigenenergies. In the case of lattice structures periodic boundaries apply, but in the case of nanoscopic systems the actual physical boundaries, determined by the shape and size of the system, are of paramount importance. In the present contribution we overview a family of boron nanoclusters, B<sub>n</sub>, with *n* ranging from 7 to 20<sup>(1-4)</sup>. These clusters exhibit a planar structure and a circular or elongated shape<sup>(5-8)</sup>. They have been the subject of extensive quantum chemical computations<sup>(9-16)</sup> and are claimed to correspond to the principal peaks in the mass spectra obtained by laser evaporation of a boron target. Evidence from photo-electron spectra<sup>(17,18)</sup> has allowed to confirm the planar structures for the mono-anions of B<sub>19</sub> and B<sub>16</sub><sup>(19-22)</sup>. In previous papers the concept of disk aromaticity<sup>(23,24)</sup> was introduced to explain the electronic structures of these nanoclusters. This approach compares the molecular orbitals of the clusters with the eigenfunctions of a particle in a circular box. We extend here this comparison to an entire series of boron clusters. The comparison also includes elongated shapes which often compete with circular shapes. So far clear quantum rules for the prediction of the bonding in these families of clusters are lacking. The aim of our comparison is to find answers to two essential questions on the structure and bonding of these nanoclusters:

- i) What is the relative importance of out-of-plane or  $\pi$ -bonding versus in-plane or  $\sigma$ -bonding?
- ii) What is the difference between bonding in clusters with elongated shapes versus disk-like clusters?

<sup>a</sup>Department of Chemistry, University of Leuven, Celestijnenlaan 200F, B-3001 Leuven, Belgium, Fax: (+32)16-327992

E-mail: arnout.ceulemans@chem.kuleuven.be

## 2. Computational Methods

Electronic structure calculations are carried out using the Gaussian09<sup>(25)</sup> suite of programs. Geometry optimization and calculation of the harmonic vibrational frequencies are performed using density functional theory (DFT) with the hybrid functional B3LYP, in conjunction with the 6-311+G(d,p)(26,27) basis set. The MO shapes of boron clusters are plotted by using the B3LYP/6-311+G(d,p) densities.

## 3. The particle on a disk model

The quantum mechanical model of a particle confined to a circular disk<sup>(28)</sup> is solved by the well known cylindrical Bessel functions. The solutions are characterized by two sets of quantum numbers: a radial quantum number,  $n = 1, 2, 3 \dots$ , referring to the order of the Bessel function, and a ring quantum number,  $m = 0, \pm 1, \pm 2 \dots$ , corresponding to the angular momentum in the plane of the disk. The ring quantum levels are usually denoted by the symbols  $\sigma, \pi, \delta, \phi, \dots$ . The eigenenergies are given by:

$$E = \frac{\hbar^2 (a_{m,n})^2}{2\mu R^2}, \text{ with: } n = 1, 2, 3, \dots \quad m = 0, \pm 1, \pm 2, \pm 3, \dots$$

where  $\mu$  is the electron mass and  $R$  is the radius of the disk. The dimensionless  $a_{m,n}$  parameters are the zeroes of the Bessel functions. The sequence of these zeroes dictates the Aufbau order of the disk waves. This order is independent of the disk radius. Table 1 reproduces a list of the lowest roots.

Table 1: The lowest  $n, m$  roots of Bessel functions

$n$	$\sigma$	$\pi$	$\delta$	$\varphi$	$\gamma$	$\eta$
1	2.4048	3.8317	5.1356	6.3802	7.5883	8.7715
2	5.5201	7.0156	8.4172	9.7610	11.0647	12.3386
3	8.6537	10.1735	11.6198	13.0152	14.3725	15.7002
4	11.7915	13.3237	14.7960	16.2235	17.6160	18.9801
5	14.9309	16.4706	17.9598	19.4094	20.8269	22.2178

The assignment of the molecular orbitals of the disk-like clusters under consideration is simply based on counting the radial and angular nodes. The number of times a function changes sign along the radius corresponds to  $n-1$ , while the number of times the sign changes upon completing a full rotation along the perimeter is equal to  $2m$ . In this way most of the MO's of our clusters could be identified unequivocally. As a result of the planar geometry of most of the structures under investigation, the MO's are divided into two separate series: in-plane ( $\sigma$ ) and out-of plane ( $\pi$ ) orbitals. The out-of-plane orbitals are based on the atomic  $2p_z$  functions on boron, while the in-plane orbitals are based on  $2s$ ,  $2p_x$ ,  $2p_y$  atomic basis functions. Both series follow the particle-on-a-disk Aufbau, implying that not only the order but also the actual energy values of DFT orbitals correlate well with the eigenenergies of the box model. The two separate series are modeled by the following parameter expressions:

$$E_{\sigma}^{n,m} = E_{\sigma}^0 + \frac{\hbar^2 (a_{m,n})^2}{2\mu R_{\sigma}^2}$$

$$E_{\pi}^{n,m} = E_{\pi}^0 + \frac{\hbar^2 (a_{m,n})^2}{2\mu R_{\pi}^2}$$

The plots of the calculated DFT orbital energies versus the corresponding  $E_{\sigma}^{n,m}$  and  $E_{\pi}^{n,m}$  are adjusted to a straight line by a least square fit, and subsequently the slope of this line is adjusted to  $45^\circ$  by adopting effective radii, labeled as  $R_{\sigma}$  and  $R_{\pi}$ . These effective radii are larger than the radius of the outer boron ring, indicating that the actual boundary of the particle waves lies beyond the outer ring.

The  $\sigma$ -orbital series starts at lower energy in view of the partial  $2s$  character. The  $E^0$  parameters are an offset which must be chosen in such a way that the  $1\sigma$  ground level of the  $\sigma$ -series in the model coincides with the DFT result. This starting point is taken as the zero-point of energy. The  $E_{\pi}^0$  parameter adjusts the  $1\sigma$  ground level of the  $\pi$ -series to the corresponding DFT result.

#### 4. The particle on a rectangle model

As mentioned planar boron clusters can also adopt a triangular array with an elongated shape. A crude but efficient quantum mechanical model for these structures is offered by the model of a particle confined to a rectangle. The solutions are characterized by two sets of quantum numbers:  $n_x$  and  $n_y$ , with  $n_x, n_y = 1, 2, 3, \dots$ . The eigenenergies are given by:

$$E_{n_x, n_y} = \frac{\hbar^2 n_x^2}{8\mu a^2} + \frac{\hbar^2 n_y^2}{8\mu b^2}$$

As before  $\mu$  is the electron mass. The  $x$ -direction is taken as the longitudinal direction, with a long-axis length  $a$ . Similarly the short-axis length along the transversal  $y$ -direction is denoted as  $b$ . Again both  $\sigma$ - and  $\pi$ -series occur. Approximate values for the effective length parameters are obtained from the main longitudinal and transversal sequences:

$$\langle a \rangle = \pi a_0 \sqrt{\frac{n_x^2 - 1}{2(E_{n_x, 1} - E_{1, 1})}}$$

$$\langle b \rangle = \pi a_0 \sqrt{\frac{n_y^2 - 1}{2(E_{1, n_y} - E_{1, 1})}}$$

where energy differences are expressed in Hartree, and  $a_0$  is the Bohr radius.

#### 5. Results

##### 5.1 Electronic structure of small disk-like boron clusters.

Boron clusters with numbers of atoms ranging from seven to twenty have been investigated. The number of the electrons – in -plane and out-of-plane – for the cluster series are shown in Table 2. Nearly for all the valence structures of  $\sigma$ -type, radial and angular disk quantum numbers can be assigned unequivocally on the basis of the orbital plots. The complete list of orbital plots for all clusters is provided in the Supporting Information. The assignments create the basis for a comparison between the particle-on-a-disk states to the orbital energies obtained from DFT calculations.

The boron clusters that will be discussed as representative examples are:  $B_7(0)$ ,  $B_{13}(+)$  (for  $B_{18}(0), B_{20}(-)$  see supplementary material). For each system we compare the  $\sigma$ - and  $\pi$ -orbital energies to the scaled eigenvalues of the particle-on-a-disk model, and show the corresponding correlation diagram. We also show MO plots of the occupied orbitals with the maximum number of cylindrical and radial quantum numbers.

## ARTICLE

Table 2. Electron distribution of valence electrons over  $\sigma$  and  $\pi$  orbitals, symmetries and energy in a.u.

Boron cluster	In-plane orbitals(Nr of Electrons)	Out-of-plane orbitals(Nr. Electrons)	Symmetry	Energy(au)	E(au)/Nr Boron atoms
B <sub>7</sub> (0)	9(18)	2(3)	C <sub>2v</sub>	-173.71022	-24.81574
B <sub>7</sub> (+)	9(18)	1(2)	C <sub>2v</sub>	-173.79753	-24.82821
B <sub>7</sub> (-)	9(18)	2(4)	C <sub>2v</sub>	-173.41786	-24.77398
B <sub>8</sub> (0)	9(18)	3(4)	D <sub>7h</sub>	-198.59679	-24.82459
B <sub>8</sub> (+)	11(22)	2(3)	C <sub>2v</sub>	-198.59619	-24.82452
B <sub>8</sub> (-)	10(20)	3(5)	C <sub>2v</sub>	-198.69938	-24.83742
B <sub>9</sub> (0)	11(21)	3(6)	C <sub>2v</sub>	-223.41003	-24.82333
B <sub>9</sub> (-)	11(22)	3(6)	D <sub>8h</sub>	-223.53574	-24.83730
B <sub>12</sub> (0)	15(30)	3(6)	C <sub>3v</sub>	-298.02690	-24.83557
B <sub>12</sub> (+)	15(29)	3(6)	C <sub>s</sub>	-297.70655	-24.80887
B <sub>12</sub> (-)	15(30)	4(7)	C <sub>s</sub>	-298.10203	-24.84183
B <sub>13</sub> (0)	16(32)	4(7)	C <sub>2v</sub>	-322.59506	-24.81500
B <sub>13</sub> (+)	16(32)	3(6)	C <sub>2v</sub>	-322.85432	-24.83494
B <sub>14</sub> (0)	16(32)	4(8)	C <sub>2v</sub>	-347.70072	-24.83576
B <sub>14</sub> (+)	16(34)	4(7)	C <sub>2v</sub>	-347.41429	-24.81530
B <sub>14</sub> (-)	16(35)	4(8)	C <sub>1</sub>	-347.72691	-24.83763
B <sub>15</sub> (0)	19(37)	4(8)	C <sub>1</sub>	-372.54513	-24.83634
B <sub>15</sub> (+)	18(36)	4(8)	C <sub>s</sub>	-372.22778	-24.81518
B <sub>15</sub> (-)	19(38)	4(8)	C <sub>1</sub>	-372.66170	-24.84811
B <sub>18</sub> (0)	23(46)	4(8)	C <sub>3v</sub>	-446.95953	-24.83108
B <sub>18</sub> (-)	23(45)	5(10)	C <sub>3v</sub>	-447.23286	-24.84627
B <sub>19</sub> (0)	23(45)	6(12)	C <sub>s</sub>	-471.95082	-24.83951
B <sub>19</sub> (-)	24(46)	6(12)	C <sub>2v</sub>	-472.10126	-24.84743
B <sub>20</sub> (-)	25(49)	6(12)	C <sub>2v</sub>	-496.91257	-24.84562
B <sub>20</sub> (2-)	25(50)	6(12)	C <sub>2v</sub>	-496.90977	-24.84548

5.1.1 B<sub>7</sub>(0):

For this system the resulting energies (in Hartree), relative to the ground root are given in Tables 3 and 4 for  $\sigma$  and  $\pi$  orbitals respectively.

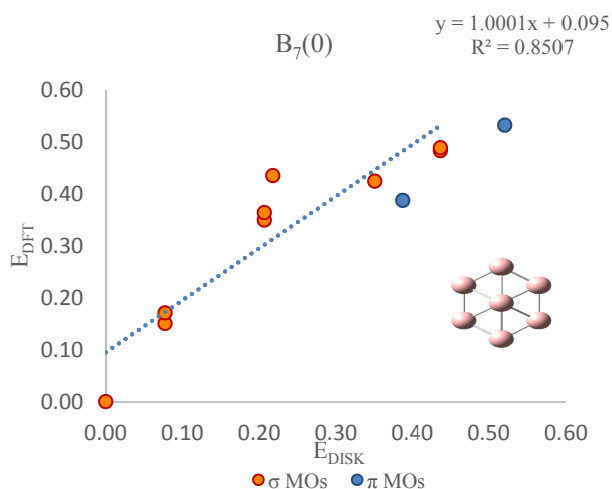
Table 3. Correlation of DFT  $\sigma$ -orbital energies and particle-on-a-disk spectrum.

B <sub>7</sub> (0)	MO	DFT		Particle in circular box	
		Label	E(Ha)	Label	E(Ha)
16	HOMO-1	2 $\pi$	0.4885	2 $\pi$	0.4364
15	HOMO-2	2 $\pi$	0.4831	1 $\varphi$	0.3509
14	HOMO-3	2 $\sigma$	0.4350	1 $\varphi$	0.3509
13	HOMO-4	1 $\varphi$	0.4241	2 $\sigma$	0.2179
11	HOMO-6	1 $\delta$	0.3638	1 $\delta$	0.2068
10	HOMO-7	1 $\delta$	0.3493	1 $\delta$	0.2068
9	HOMO-8	1 $\pi$	0.1706	1 $\pi$	0.0774
8	HOMO-9	1 $\pi$	0.1505	1 $\pi$	0.0774
7	HOMO-10	1 $\sigma$	0.0000	1 $\sigma$	0.0000

The correlation between DFT and scaled model energies is shown in Figure 1, while Figure 2 provides orbital plots of the orbitals with maximal numbers of nodes.

Table 4. Correlation of DFT  $\pi$ -orbital energies and particle-on-a-disk spectrum

B <sub>7</sub> (0)	MO	DFT		Particle in a circular box	
		Label	E(Ha)	Label	E(Ha)
17	HOMO	1 $\pi$	0.5321	1 $\pi$	0.5321
12	HOMO-5	1 $\sigma$	0.3874	1 $\sigma$	0.3874

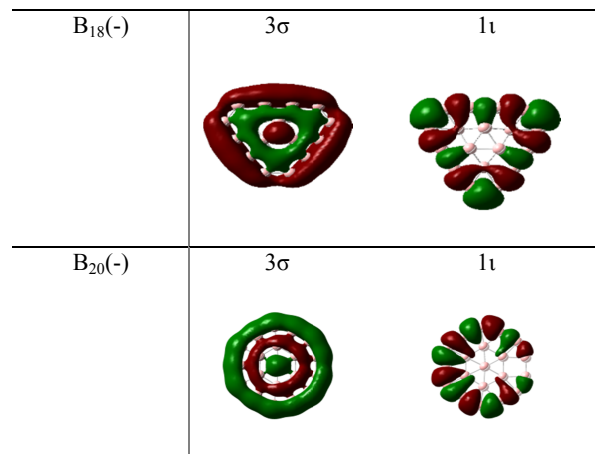
Figure 1:  $B_7(0)$ : DFT versus disk model energies.

The highest occupied  $n\sigma$ -orbital is the  $2\sigma$ -orbital with one radial node, between the central atom and the outer hexagon (see Figure 2). On the central atom some further  $2p_z$ -character is noted which is due to a slight out-of-plane movement of the central atom. The maximal number of angular nodes corresponds to three in the  $1\pi$  orbital, which consists of a perfect sign alternation in every atom of the outer ring.

### 5.1.2 $B_{13}(0)$ :

The neutral  $B_{13}$  cluster consists of an inner triangle, surrounded by an outer ring of ten atoms. The energy correlations (in Hartree), relative to the ground root are given in Tables 5 and 6 for  $\sigma$  and  $\pi$  orbitals respectively.

	Max number of rings	Max number of nodes
$B_7(0)$	$2\sigma$	$1\phi$
$B_{13}(0)$	$3\sigma$	$1\eta$

Figure 2.  $B_7(0)$ ,  $B_{13}(0)$ ,  $B_{18}(-)$ ,  $B_{20}(-)$ : orbitals with maximal  $n$  and maximal  $m$ Table 5. Correlation of DFT  $\sigma$ -orbital energies and particle-on-a-disk spectrum.

$B_{13}(0)$	MO	DFT		Particle in a circular box	
		Label	E(Ha)	Label	E(Ha)
32	HOMO-1	$2\delta$	0.4975	$1\eta$	0.4534
31	HOMO-2	$2\delta$	0.4775	$3\sigma$	0.4403
28	HOMO-5	$3\sigma$	0.4411	$2\delta$	0.4146
27	HOMO-6	$2\pi$	0.4198	$2\delta$	0.4146
26	HOMO-7	$2\pi$	0.4029	$1\gamma$	0.3300
24	HOMO-9	$1\eta$	0.3828	$1\gamma$	0.3300
23	HOMO-10	$1\gamma$	0.3789	$2\pi$	0.2767
22	HOMO-11	$1\gamma$	0.3786	$2\pi$	0.2767
21	HOMO-12	$1\phi$	0.3136	$1\phi$	0.2225
20	HOMO-13	$1\phi$	0.2847	$1\phi$	0.2225
19	HOMO-14	$2\sigma$	0.1875	$2\sigma$	0.1382
18	HOMO-15	$1\delta$	0.1785	$1\delta$	0.1312
17	HOMO-16	$1\delta$	0.1745	$1\delta$	0.1312
16	HOMO-17	$1\pi$	0.0796	$1\pi$	0.0491
15	HOMO-18	$1\pi$	0.0693	$1\pi$	0.0491
14	HOMO-19	$1\sigma$	0.0000	$1\sigma$	0.0000

Table 6. Correlation of DFT  $\pi$ -orbital energies and particle-on-a-disk spectrum.

$B_{13}(0)$	MO	DFT		Particle in a circular box	
		Label	E(Ha)	Label	E(Ha)
33	HOMO	$1\delta$	0.5563	$1\delta$	0.5563
30	HOMO-3	$1\pi$	0.4634	$1\pi$	0.4634
29	HOMO-4	$1\pi$	0.4623	$1\pi$	0.4623
15	HOMO-8	$1\sigma$	0.4010	$1\sigma$	0.4010

The energy correlation plot is presented in Figure 3. A typical feature of this plot, which could also already be observed for the  $B_7$  cluster (Figure 1), is the change of the slope at about 0.30 Hartree. This change reflects roughly a transition from orbitals that are predominantly of  $2s$  character to orbitals with a predominant  $2p$  character. We will return to this feature in the discussion of the radial scaling factors. Figure 2 displays the  $3\sigma$

orbital and  $1\eta$  orbital, having two radial and five angular nodes resp.

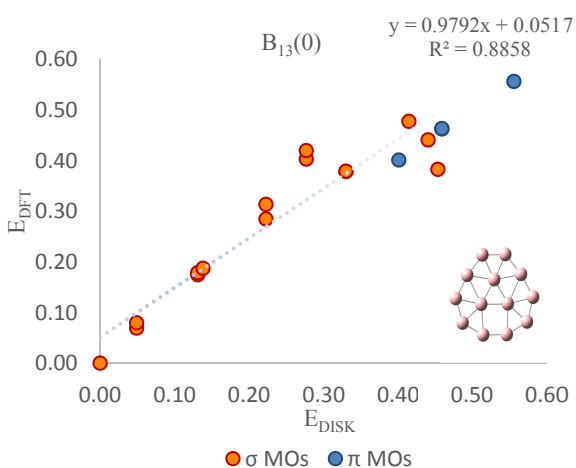


Figure 3.  $B_{13}(0)$ : correlation between DFT orbital energies and particle-on-a-disk spectrum

### 5.2 Rescaled radii

As we explained in the section on the disk model, the fit with the DFT results required a rescaling to an effective radius in the model treatment, as compared with the actual radius of the outer ring. This rescaling had to be carried out independently for the  $\sigma$  and  $\pi$  series. The results are listed in table 7. The radii always increase as compared to the actual cluster radius. The extension in the table indicated the increase of the disk radius as compared to the actual cluster radius.

Table 7. Rescaled radii ( $\text{\AA}$ ) and extension ( $\text{\AA}$ ) for the  $\sigma$  and for the  $\pi$  band of clusters

Cluster	$R\sigma$	Extension	$R\pi$	Extension
$B_7(0)$	7.94	4.54	5.81	2.41
$B_7(-)$	7.11	3.71	6.79	3.39
$B_8(0)$	7.06	3.66	5.56	2.16
$B_8(+)$	6.83	3.43	4.97	1.57
$B_8(-)$	7.18	3.78	6.08	2.68
$B_9(0)$	7.34	3.94	5.88	2.48
$B_9(-)$	7.31	3.91	5.86	2.46
$B_{12}(0)$	6.45	3.05	4.92	1.52
$B_{12}(+)$	6.25	2.85	4.68	1.28
$B_{12}(-)$	6.85	3.45	3.81	0.41
$B_{13}(0)$	6.30	2.90	5.81	2.41
$B_{13}(+)$	6.20	2.80	4.70	1.30
$B_{14}(0)$	6.13	2.73	5.67	2.27
$B_{14}(+)$	6.18	2.78	6.36	2.96
$B_{14}(-)$	6.28	2.88	5.52	2.12
$B_{15}(0)$	6.19	2.80	5.99	2.59
$B_{15}(+)$	5.88	2.48	5.99	2.59
$B_{15}(-)$	6.27	2.87	6.30	2.90
$B_{18}(0)$	5.50	2.10	4.52	1.12
$B_{18}(-)$	5.60	2.20	4.72	1.32
$B_{19}(0)$	5.90	2.50	4.81	1.40
$B_{19}(-)$	6.10	2.70	6.22	3.40
$B_{20}(-)$	5.99	2.59	4.79	1.39
$B_{20}(-2)$	5.85	2.45	5.33	1.93

This result shows several interesting features. In most cases the radius increases with increasing cluster charge, as should be expected for electron clouds with increasing number of electrons. Also the extension of the  $\pi$ -cloud is always smaller than the extension of the  $\sigma$ -cloud. This can be linked to the radial extension of the corresponding basic orbitals. The  $\pi$ -band is based on the  $2p_z$  orbitals with a smaller radial extension as compared to the  $2p_x$ ,  $2p_y$  orbitals involved in the  $\sigma$ -band. According to the quantum particle in a box models the extension of the box usually corresponds to one bond length, which for a typical BB bond length of 1.6-1.7  $\text{\AA}$ . The  $\sigma$ -extensions are larger than this distance, while the  $\pi$ -extensions are mostly somewhat smaller.

### 5.3 Electronic structure of elongated clusters

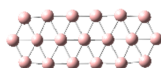
For many clusters one finds competing minimal energy structures with elongated and circular shapes. The most regular elongated shapes correspond to a double stripe of boron triangles, with a cap at each end. We have studied in detail the electronic levels of the  $B_{16}(0)$  (supplementary material) and  $B_{19}(-)$  clusters as compared to the particle in a rectangular box model. The actual structures show small deviations from planarity. Both clusters were made planar in order to remove some residual  $\sigma$ - $\pi$  hybridization.

#### Elongated $B_{19}(-)$ :

In Table 8, we provide the orbital energies for the  $B_{19}(-)$  cluster. Here the highest value for the long-axis quantum number is 7, but the short-axis quantization remains 4. As in  $B_{16}(0)$  there are two orbitals with strong localization on the caps which cannot be assigned with rectangular quantum numbers. These are the HOMO-4 and HOMO-5.

Table 8. Orbital energies (Hartree), and rectangular quantum numbers

$B_{19}(-)$					
$\sigma$	Label	$E(\text{Ha})$	$\pi$	Label	$E(\text{Ha})$
HOMO-2	3,4	0.58643	HOMO	2,2	0.65794
HOMO-4	?	0.52649	HOMO-1	4,1	0.62174
HOMO-5	?	0.50234	HOMO-3	1,2	0.54019
HOMO-6	2,4	0.46257	HOMO-7	3,1	0.45739
HOMO-8	7,2	0.39228	HOMO-11	2,1	0.30093
HOMO-9	6,2	0.39037	HOMO-16	1,1	0.23353
HOMO-10	1,4	0.32676			
HOMO-12	4,3	0.25920			
HOMO-13	3,3	0.26929			
HOMO-14	7,1	0.26905			
HOMO-15	2,3	0.23978			
HOMO-17	1,3	0.23270			
HOMO-18	5,2	0.22623			
HOMO-19	4,2	0.21467			
HOMO-20	6,1	0.20637			
HOMO-21	5,1	0.18097			
HOMO-22	3,2	0.17731			
HOMO-23	2,2	0.16142			
HOMO-24	4,1	0.15832			
HOMO-25	1,2	0.13871			
HOMO-26	3,1	0.12752			
HOMO-27	2,1	0.09924			
HOMO-28	1,1	0.09435			



In Figure 4, we plot for both clusters the energy difference in the principal series,  $E(n_x, 1) - E(1, 1)$ , in the  $\sigma$ - and the  $\pi$ -band. The plots are surprisingly linear in spite of the crude model. As can be seen from the figure the slopes for the  $\sigma$ -band are much less pronounced than for the  $\pi$ -band. This is also reflected by the effective radii as given in Table 9. In comparison to the actual atomic lengths of the long and short axis it is remarkable that the  $\sigma$ -fit highly overestimates the actual size, while for the  $\pi$ -parameters it is rather the opposite. This is probably related to the mixed orbital character of the  $\sigma$ -orbitals which contain the  $2p_x$  and  $2p_y$  orbitals with intrinsic nodal properties.

In Figure 5 orbital plots are provided for the highest orbitals of the  $(n_x, 1)$  and  $(1, n_y)$  principal series.

Table 9. Effective radii (in Å) for elongated clusters, as compared to the atomic distances along the long and short axis

	$B_{16}(0)$		$B_{19}(-)$	
	$\langle a \rangle$	$\langle b \rangle$	$\langle a \rangle$	$\langle b \rangle$
$\sigma$	16.56	9.06	19.21	9.55
$\pi$	7.37	3.66	7.38	3.67
Actual sizes	a	b	a	b
	7.92	3.32	9.47	3.12

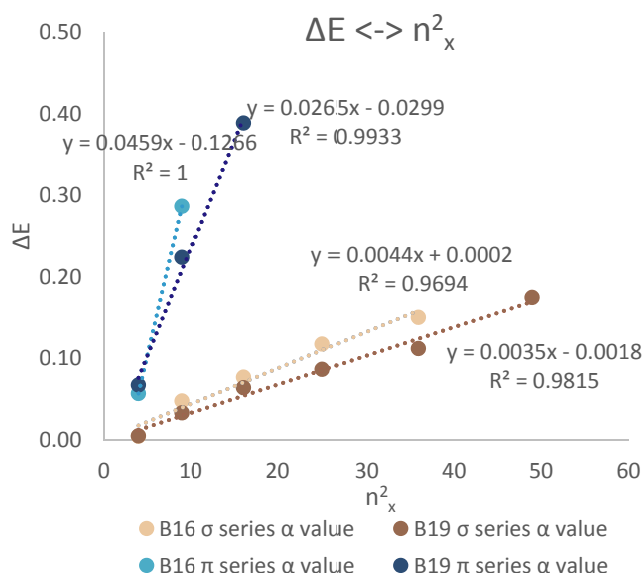


Figure 4. Energy difference,  $\Delta E = E(n_x, 1) - E(1, 1)$ , in the  $\sigma$ - and the  $\pi$ -band for both elongated structures.

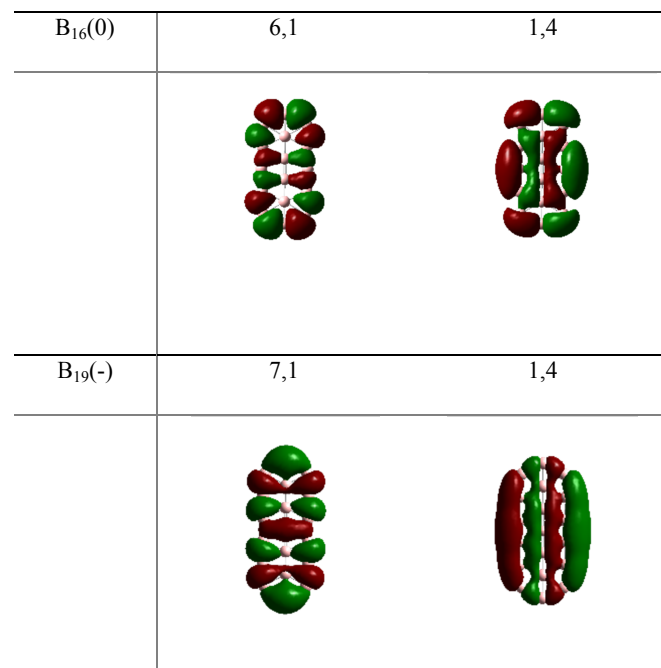


Figure 5. Terminal orbitals of the principal series  $(n_x, 1)$  and  $(1, n_y)$

## 6. Discussion

### 6.1 Molecular structures

Planar and quasiplanar oligomers of boron essentially present two types of geometries: circular disks and elongated stripes. It is tempting to relate the growth patterns of these two kinds to the existence of two kinds of larger 3D clusters: the disks may

be curved to form calixarenes and eventually boron fullerenes, while the stripes may roll up to form cylinders.

Most of the clusters display a triangulated disk structure, and may be viewed as tessellations of the triangulated plane. The ring of nearest neighbours encircling a triangle in such a plane contains 9 atoms. The general rule applies that an inner ring of  $n$  atoms is surrounded by an outer ring of  $n+6$  atoms. In Figure 8 we apply this rule to the planar structures we have studied. Examples which strictly obey this geometrical rule are  $B_8$ ,  $B_{12}$ , and  $B_{18}$ . Larger clusters are frequently characterized by the presence of open faces: as an example  $B_{34}$  has a coronene-like shape with an open pentagon in the middle, surrounded by a triangulated strip. For  $B_{14}$  the minimal energy search generates a geometry with an inner rhombus with 4 atoms, surrounded by a ring of 10, but this competes with an elongated shape and a non-planar isomer. A similar situation occurs for  $B_{16}$ . The triangulated shape with an inner part of 5 atoms and surrounded by an 11-ring is expected for  $B_{16}$ , but again such a shape is less stable than an elongated form.

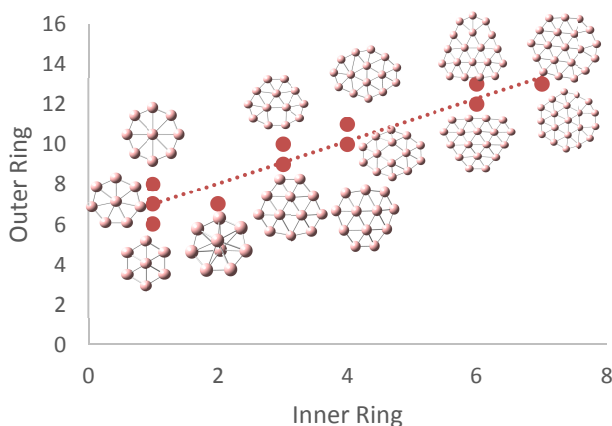


Figure 6. Triangulated disks: number of outer atoms versus number of inner atoms. The line corresponds to the  $n+6$  relation.

## 6.2 Quantum rules for the $\sigma$ subband

For ideal planar structures there is a strict separation of  $\sigma$  and  $\pi$  orbitals on the basis of reflection symmetry through the molecular plane. Each kind thus forms a separate subband for which specific quantum rules can be expressed.

For the  $\sigma$  subband, there are two maximal node principles:

a) The modes with the highest value for the angular momentum depend on the number of atoms in the outer ring. If this number is equal to  $2m$ , there is one occupied orbital transforming as  $\cos(m\varphi)$ . If this number is odd,  $2m+1$ , there is a pair of cyclic orbitals, transforming as  $\cos(m\varphi)$  and  $\sin(m\varphi)$ . While these functions thus have a total of  $2m$  angular nodes, they are nonetheless bonding combinations, because they consist of tangential  $2p$  orbitals. These basis functions change sign at the atomic positions, but form bonding combinations at the

interatomic positions. The radial quantum number for these modes is equal to one ( $n=1$ ) indicating that there are no radial nodes.

b) Vice-versa the highest radial quantum number for orbitals without angular nodes is equal to the number of concentric rings plus one. An atom in the center should not be counted in. As an example for a structure such as  $B_{12}$ , consisting of a triangle surrounded by a nonagon, there are two concentric rings. The highest  $n\sigma$  orbital thus has  $n = 2 + 1 = 3$ .

Both these orbital characteristics refer to modes that are fully delocalized over the disk. In order to understand these features one should make the comparison with a valence bond model for these boron compounds. The boron element is 'electron deficient' in the sense that it has only 3 valence electrons for four valence orbitals. As a result it must recur to multi-center two-electron bonding. Using the adaptive natural density partitioning method (ANDP)(29–31) Boldyrev et al. have concluded a localized description of the valence bond in the boron disk, based on two bond-types: i) the peripheral ring is always completely bonding with localized 2c-2e bonds, ii) the interior of the disk is held together by distributed triangular 3c-2e bonds. The latter bonding type is characteristic of the borane compounds as well and directly follows from the electron-deficiency of boron. Remarkably 4-centre bonds on open squares in the interior are never found. From an overview of the cluster series, it can be inferred that the triangle bonds form an alternating network, so that approximately only half of the triangles are covered. As a simple example we may consider the  $B_7^+$  cation. This cluster contains 20 valence electrons, two of which belong to the  $\pi$ -band. Of the remaining 18 electrons not less than 12 are invested in forming a fully bonding outer hexagon with six 2c-2e bonds. Then six electrons remain which can account for three triangular bonds; this is half the number of interior triangles in this structure. This distribution of 3c-2e in the interior in a sense corresponds to a Kekule symmetry breaking, giving rise to resonance delocalization.

The existence of a fully bonding perimeter is a remarkable feature of these boron clusters. It directly confirms our initial hypothesis that for these small clusters the confinement by the atomic boundary is the dominant feature of the structure. The highest angular node orbital which is present in all structures is connecting all the outer atoms through the tangential  $2p$  orbitals on the peripheral atoms and is a direct consequence of the electron precise bonding around the outer ring. Likewise the highest radial node of  $n\sigma$ -type realizes a fully bonding combination of  $2s$  and radial  $2p$  orbitals of the outer atoms. Such an orbital can be combined with a similar bonding mode on the inner part to form an in-phase all bonding orbital and an out-of-phase orbital with a radial node. If the inner part only consists of one atom, this is not possible since the out-of-phase combination would not have an interior bonding part, hence the rule that an atom in the center does not count.

### 6.3 Quantum rules for the $\pi$ subband

It seems that the formation of the in-plane  $\sigma$ -frame is the determining step for the allocation of the number of  $\sigma$ -electrons. The surplus is then assigned to the  $\pi$  subband. One indication for this hypothesis is that the HOMO frequently (but not always) is of  $\pi$ -type. The number of occupied levels of the  $\pi$  subband is a slowly but steadily rising function of nuclearity (see Table 1). It is clear that this subband consists of highly delocalized orbitals which are distributed over the framework and form a slowly increasing series, which basically only depends on the shape and size of the cluster, and not on the detailed structure. This explains why an analogy could be drawn with conjugated planar carbon systems, which are not isoelectronic but only analogous as far as shape and size are concerned. For circular shapes the  $\pi$ -orbitals are close to the solutions of the disk model, while for elongated shapes the simple model of a particle in a narrow rectangular box is already sufficient.

### 6.3 Elongated structures

A crude rectangular box model was found to be able to rationalize the orbital shapes in the elongated structures, except for a pair of orbitals which were strongly localized on the capping regions, at both ends of the longitudinal axis. For the  $\sigma$  subband the maximal number of nodes in the transversal direction cannot be greater than four. This corresponds to three nodal planes which are coincident with the three arrays of the nuclear positions. These modes are indeed realized by combinations of the  $2p_y$ -orbitals which define nodal planes through the nuclear positions. In the longitudinal direction the highest quantum number is 6 for  $B_{16}$  and 7 for  $B_{19}$ . This count depends on the number of atoms along the perimeter, not taking into account the capping atoms. In this way one counts 10 perimeter atoms for  $B_{16}$ , and 12 for  $B_{19}$ . Combinations of in-plane orbitals which are nodal at these atoms indeed yield the (6,1) and (7,1) orbitals shown in Figure 5.

## 7. Conclusions

In this article free-particle models have been considered in order to obtain quantum rules for boron clusters with nuclearities from seven to twenty. In view of the near-planarity of the clusters the electronic structure separates into  $\sigma$  and  $\pi$  subbands. These incorporate different bonding rules.

As for the in-plane  $\sigma$ -bonding, since boron is electron deficient it cannot form electron-precise bonds. Quite remarkably it nevertheless invests sufficient electron pairs to form a closed ring of electron-precise bonds around the full perimeter of the cluster. The remaining  $\sigma$ -orbitals form a triangulated network of 3c-2e bonds corresponding approximately to half the number of triangles inside. As an example, in  $B_{20}(2-)$ , there are 25 occupied  $\sigma$ -orbitals, 13 of which are needed for the perimeter bonding. The inner structure contains 23 triangles and one square. The remaining 12 orbitals will form delocalized bonds

over this inner network, in approximate agreement with half the number of triangles. This bonding scheme is confirmed by the particle-on-disk model in that the highest angular momentum mode is dictated by the number of bonds in the outer ring. If this number is even,  $2m$ , there is one occupied orbital transforming as  $\cos(m\phi)$ . If the number is odd,  $2m+1$ , there is a pair of cyclic orbitals transforming as  $\cos(m\phi)$  and  $\sin(m\phi)$ . Moreover, the highest radial quantum number is equal to the number of concentric rings plus one (atoms in the center should not be counted in). The remarkable feature of the disk model is that it not only accounts for the Aufbau of the  $\sigma$ -subband, but that there is also a semi-quantitative correspondence. This is the more remarkable, since the orbital basis consists of  $2s$  and  $2p_{x,y}$  orbitals with different nodal characteristics. However both orbital types hybridize so as to form the waves that are characteristic for a particle in a disk. Of course towards the frontier region of the band, the actual molecular geometry becomes more important and deviations from the model start to show up.

The  $\pi$  subband has different characteristics. The orbitals are much more delocalized, forming shells which principally depend on the overall size of the system. As can be seen the electron counts corresponding to the quantum rule for this subband tend to comply with the shell structure of the disk model, and are to be considered as the magic numbers of *disk aromaticity*. The smaller clusters in Table 2 often have 6  $\pi$ -electrons corresponding to the usual aromatic  $(1\sigma)^2(1\pi)^4$  sextet, while larger clusters have a preference for 12  $\pi$ -electrons, occupying  $(1\sigma)^2(1\pi)^4(1\delta)^4(2\sigma)^2$ .

In conclusion our systematic study of planar boron clusters at low nuclearities has provided rules that apparently dictate the bonding. They provide an answer to the first question in the introduction, concerning the relationship between the in-plane and out-of-plane subbands. In contrast the second question on the relationship between elongated and circular isomers does not seem to receive a clear answer, since both alternatives can be very close in energy, and the boron valence shell shows enough flexibility to adapt to both bonding topologies.

## 8. Acknowledgements

A.G.A would like to thank the FWO for financial support.

## 9. Notes and references

Electronic Supplementary Information (ESI) available: orbital plots, assignment tables and correlation diagrams, and xyz coordinates for all clusters listed in Table 2.

1. Tai TB, Tam NM, Nguyen MT. Structure of boron clusters revisited,  $B_n$  with  $n = 14-20$ . Chem Phys Lett. 2012, 30(0):71-6.
2. Aihara J, Kanno H, Ishida T. Aromaticity of Planar Boron Clusters Confirmed. J Am Chem Soc. 2005, 127(38):13324-30.

- Tai T, Tam N, Nguyen M. The Boron conundrum: the case of cationic clusters  $B_n^+$  with  $n = 2-20$ . *Theor Chem Acc*. 2012, 131(6):1-15.
- Nguyen MT, Matus MH, Ngan VT, Grant DJ, Dixon DA. Thermochemistry and Electronic Structure of Small Boron and Boron Oxide Clusters and Their Anions. *J Phys Chem A*. 2009, 113(17):4895-909.
- Pham HT, Duong LV, Pham BQ, Nguyen MT. The 2D-to-3D geometry hopping in small boron clusters: The charge effect. *Chem Phys Lett*. 2013, 577(0):32-7.
- Oger E, Crawford NRM, Kelting R, Weis P, Kappes MM, Ahlrichs R. Boron Cluster Cations: Transition from Planar to Cylindrical Structures. *Angew Chem Int Ed*. 2007, 46(44):8503-6.
- Sergeeva AP, Popov IA, Piazza ZA, Li W-L, Romanescu C, Wang L-S, et al. Understanding Boron through Size-Selected Clusters: Structure, Chemical Bonding, and Fluxionality. *Acc Chem Res*. 2014, 47(4):1349-58.
- Kiran B, Bulusu S, Zhai H-J, Yoo S, Zeng XC, Wang L-S. Planar-to-tubular structural transition in boron clusters:  $B_{20}$  as the embryo of single-walled boron nanotubes. *Proc Natl Acad Sci U S A*. 2005, 102(4):961-4.
- Kawai R, Weare JH. Anomalous stability of  $B_{13}^+$  clusters. *Chem Phys Lett*. 1992, 191(3-4):311-4.
- Aihara J.  $B_{13}^+$  Is Highly Aromatic. *J Phys Chem A*. 2001, 105(22):5486-9.
- Boustani I. Systematic LSD investigation on cationic boron clusters:  $B_n^+$  ( $n=2-14$ ). *Int J Quantum Chem*. 1994, 52(4):1081-111.
- Fowler JE, Ugalde JM. The Curiously Stable Cluster and its Neutral and Anionic Counterparts: The Advantages of Planarity. *J Phys Chem A*. 1999, 104(2):397-403.
- Fowler PW, Gray BR. Induced Currents and Electron Counting in Aromatic Boron Wheels:  $B_8^{2-}$  and  $B_9^-$ . *Inorg Chem*. 2007, 46(7):2892-7.
- Zhai H-J, Alexandrova AN, Birch KA, Boldyrev AI, Wang L-S. Hepta- and Octacoordinate Boron in Molecular Wheels of Eight- and Nine-Atom Boron Clusters: Observation and Confirmation. *Angew Chem Int Ed*. 2003, 42(48):6004-8.
- Lin L, Lievens P, Nguyen MT. In search of aromatic seven-membered rings. *Concept Asp Electron Densities Density Funct*. 2010, 943(1-3):23-31.
- Kiran B, Gopa Kumar G, Nguyen MT, Kandalam AK, Jena P. Origin of the Unusual Stability of  $B_{12}$  and  $B_{13}^+$  Clusters. *Inorg Chem*. 2009, 48(21):9965-7.
- Alexandrova AN, Zhai H-J, Wang L-S, Boldyrev AI. Molecular Wheel  $B_8^{2-}$  as a New Inorganic Ligand. *Photoelectron Spectroscopy and ab Initio Characterization of  $LiB_8^-$* . *Inorg Chem*. 2004, 43(12):3552-4.
- Alexandrova AN, Boldyrev AI, Zhai H-J, Wang L-S. All-boron aromatic clusters as potential new inorganic ligands and building blocks in chemistry. *Coord.Chem.Rev*. 2006, 250(21-22):2811-66.
- Huang W, Sergeeva AP, Zhai H-J, Averkiev BB, Wang L-S, Boldyrev AI. A concentric planar doubly  $\pi$ -aromatic  $B_{19}^-$  cluster. *Nat Chem*. 2010, 2(3):202-6.
- Jiménez-Halla JOC, Islas R, Heine T, Merino G.  $B_{19}^-$ : An Aromatic Wankel Motor. *Angew Chem Int Ed*. 2010, 49(33):5668-71.
- Sergeeva AP, Zubarev DY, Zhai H-J, Boldyrev AI, Wang L-S. A Photoelectron Spectroscopic and Theoretical Study of  $B_{16}^-$  and  $B_{16}^{2-}$ : An All-Boron Naphthalene. *J Am Chem Soc*. 2008, 130(23):7244-6.
- Merino G, Heine T. And Yet It Rotates: The Starter for a Molecular Wankel Motor. *Angew Chem Int Ed*. 2012, 51(41):10226-7.
- Tai TB, Havenith RWA, Teunissen JL, Dok AR, Hallaert SD, Nguyen MT, et al. Particle on a Boron Disk: Ring Currents and Disk Aromaticity in  $B_{20}^{2-}$ . *Inorg Chem*. 2013, 52(18):10595-600.
- Tai TB, Ceulemans A, Nguyen MT. Disk Aromaticity of the Planar and Fluxional Anionic Boron Clusters  $B_{20}^{2-}$ . *Chem - Eur J*. 2012, 18(15):4510-2.
- Frisch MJ, Trucks GW, Schlegel HB, Scuseria GE, Robb MA, Cheeseman JR, et al. *Gaussian 09, Revision A.1*. Wallingford, CT: Gaussian, Inc.; 2009.
- Becke AD. Density-functional thermochemistry. III. The role of exact exchange. *J Chem Phys*. 1993, 98(7):5648-52.
- Becke AD. A new mixing of Hartree-Fock and local density-functional theories. *J Chem Phys*. 1993, 98(2):1372-7.
- Robinett RW. Visualizing the solutions for the circular infinite well in quantum and classical mechanics. *Am J Phys*. 1996, 64(4):440-6.
- Zubarev DY, Boldyrev AI. "Developing paradigms of chemical bonding: adaptive natural density partitioning. *Phys Chem Chem Phys*. 2008, 10(34):5207-17.
- Zubarev DY, Boldyrev AI. Revealing Intuitively Assessable Chemical Bonding Patterns in Organic Aromatic Molecules via Adaptive Natural Density Partitioning. *J Org Chem*. 2008, 73(23):9251-8.
- Zubarev DY, Boldyrev AI. Comprehensive analysis of chemical bonding in boron clusters. *J Comput Chem*. 2007, 28(1):251-68.